Self-Assembly of H-Bonded Side-Chain and Cross-Linking Copolymers Containing Diblock-Copolymeric Donors and Single/Double H-Bonded Light-Emitting Acceptors

HONG-CHEU LIN, MENG-DAN JIANG, SHEN-CHANG WU, LENG-LONG JOU, KAI-PIN CHOU, CHING-MAO HUANG, KUNG-HWA WEI

Department of Materials Science and Engineering, National Chiao Tung University, Hsinchu, Taiwan, Republic of China

Received 1 April 2009; accepted 12 May 2009
DOI: 10.1002/pola.23521
Published online in Wiley InterScience (www.interscience.wiley.com).

ABSTRACT: A series of diblock-copolymers were synthesized through anionic polymerization of styrene and *tert*-butyl methacrylate (tBuA) with different monomer ratios, and analogous block-copolymeric derivatives **(PS-*b*-PAA)s** with monofunctional carboxylic acid groups were obtained by further hydrolyzation as hydrogen-bonded (H-bonded) proton donors. Via H-bonded interaction, these diblock-coplymeric donors **(PS-*b*-PAA)s** were incorporated with luminescent mono-pyridyl/bis-pyridyl acceptors to form single/double H-bonded supramolecules, that is, H-bonded side-chain/cross-linking copolymers, respectively. The supramolecular architectures formed by donor polymers and light-emitting acceptors were influenced by the ratio of acid blocks in the diblock copolymeric donors and the type of single/double H-bonded light-emitting acceptors. Their thermal and luminescent properties can be adjusted by H-bonds, and more than 100 nm of red-shifted photoluminescence (PL) emissions were observed, which depend on the degrees of the H-bonding interactions. Self-assembled phenomena of amphiphilic dibolck copolymers and their H-bonded complexes were confirmed by TEM micrographs, and supramolecular microphase separation of spherical micelle-like morphology was demonstrated to affect the photophysical properties. Polymer light-emitting diode (PLED) devices containing H-bonded complexes showed electroluminescence (EL) emissions of 503–560 nm under turn-on voltages of 7.5–9.0 V, maximum power efficiencies of 0.23–0.37 cd/A (at 100 mA/cm^2), and maximum luminances of 318–519 cd/m^2 (around 25 V). © 2009 Wiley Periodicals, Inc. J Polym Sci Part A: Polym Chem 47: 4685–4702, 2009

Keywords: diblock copolymer; luminescence; supramolecular structures

INTRODUCTION

Fascinating subjects in areas such as materials science, nanochemistry, and biomimetic chemistry are concerned with the creation of supramolecular architectures with well-defined shapes and functions, where self-assembly of molecules through noncovalent forces including hydrophobic and hydrophilic effects,[1] hydrogen bonding,[2] metal-ligand interactions,[3] microphase segregation, and shape effects[4] are involved. With regard to microphase segregation, block copolymers are utilized to generate a variety of different morphologies, namely sphere, cylinder, and lamellae, due to the microscopic phase separation in solid state and selective solvation in solutions, which provide an

Additional Supporting Information may be found in the online version of this article.

Correspondence to: H.-C. Lin (E-mail: linhc@mail.nctu.edu.tw)

Journal of Polymer Science: Part A: Polymer Chemistry, Vol. 47, 4685–4702 (2009)

attractive route to nanostructures. In particular, hydrogen bonding has also been applied to produce packed nanohelical polymer structures,[5–7] core-shell micelle architectures,[8–14] and liquid-crystalline assemblies.[15–20] Therefore, noncovalent interactions of H-bonds are combined with covalent chemistry in order to construct new supramolecular polymers.

For example, the hydrogen bonds formed between pyridines and carboxylic acids have been shown to be beneficial for spontaneous construction of supramolecular structures.[18] Hawker and coworkers also demonstrated block copolymer lithography yielding nanometer-sized hexonal structures by hierarchical self-assembly of H-bonding.[21] Zhang et al. prepared the core-shell-corona micelles from the complexation between core-shell micelles of polystyrene-*block*-poly(acrylic acid) (**PS-*b*-PAA**) and a double hydrophilic diblock copolymer of poly(ethylene glycol)-*block*-poly(4-vinyl pyridine).[22,23] Peng et al. studied the complexation of polystyrene-*block*-poly(4-vinyl pyridine) with linear aliphatic acids in chloroform indicating the resulting complexes may generate self-assembly of nanosized vesicles or molecularly dispersed state, corresponding to the length of the aliphatic chains.[11] **PS-*b*-PAA** is a typical cross-linked and amphiphilic block copolymer,[24–26] whose self-assemblies into core-shell nanomicelles have been extensively studied for the construction of supramolecules. It was also applied by Taton et al. to demonstrate an alternative and noncovalent method of modifying single-walled carbon nanotubes by encasing the nanotubes within copolymer micelles of cross-linked **PS-*b*-PAA**.[27]

In our previous work,[18,28] several series of liquid crystalline and light-emitting supramolecular assemblies were constructed by complexation of two complementary components containing various functional proton donors and acceptors. The mesogenic and photoluminescence (PL) properties of the functional cores can be adjusted not only by the chemical structures of the cores but also by their surrounding proton donors or acceptors, and their H-bonded effects on photoluminescent supramolecules have been investigated previously. In contrast, block copolymers have been rarely considered as optical tuning materials for chromophores and relatively few researches regarding their functions as optical wave-adjusting materials have been explored and evaluated. For instance, Jenekhe et al. reported that block copolymers with light-emitting (phenyl-quinoline, PPQ) blocks can form the morphology of self-organized hollow spherical micelles in the dimension of micrometers.[29] Moreover, the refractive-index of nanocomposites can be tuned by inclusion of nanoparticles in the nano-tailored matrices of block-copolymers.[30] In this study, the self-assembled matrices of micellar diblock copolymers, that is, polystyrene-*block*-poly(acrylic acid)s **(PS-*b*-PAA)s**, were hydrolyzed from diblock copolymers, that is, polystyrene-*block*-poly(*tert*-butyl acrylate)s **(PS-*b*-P*t*BuA)s**, in which tert-butyl acrylate groups were turn into acrylic acid groups by the hydrolysis reaction. Accordingly, a series of photoluminescent molecules containing mono- and bis-pyridyl moieties were designed to complex with amphiphilic diblock copolymers **(PS-*b*-PAA)s** to form single/double H-bonded complexes, that is, supramolecular side-chain/cross-linking polymers (as shown in Fig. 1), respectively. Therefore, H-bonded effects on the self-assembled and PL properties of these supramolecules in solid state are illustrated.

EXPERIMENTAL

Measurements and Characterization

^{1}H NMR spectra were recorded on a Varian Unity 300 MHz spectrometer using $CDCl_3$ or DMSO-d_6 solvent with tetramethyl silane as a reference. Elemental analyses were performed on a HERAEUS CHN-OS RAPID elemental analyzer. Fourier transform infrared (FTIR) spectra were performed on a Nicolet 360 FTIR spectrometer. Phase transition temperatures were determined by differential scanning calorimetry (Perkin-Elmer Diamond) with a heating and cooling rate of 10 °C/min and polarizing optical microscope (Leica DMLP) equipped with a hot stage. Thermogravimetric analyses (TGA) were conducted on a Du Pont Thermal Analyst 2100 system with a TGA 2950 thermogravimetric analyzer at a heating rate of 10 °C/min under nitrogen. UV-visible (UV-vis) absorption spectra were recorded in dilute THF solutions (10^{-6} M) on a HP G1103A spectrophotometer, and PL spectra were obtained on a Hitachi F-4500 spectrophotometer. Thin films of UV-vis and PL measurements were spin-coated on quartz substrates from THF solutions with a concentration of 1 wt %. Transmission electron microscopy (TEM) images were obtained by a Hitachi H-600 microscope. All TEM samples were stained with iodine and prepared from solutions in chlorobenzene with a concentration of 0.2 wt %.

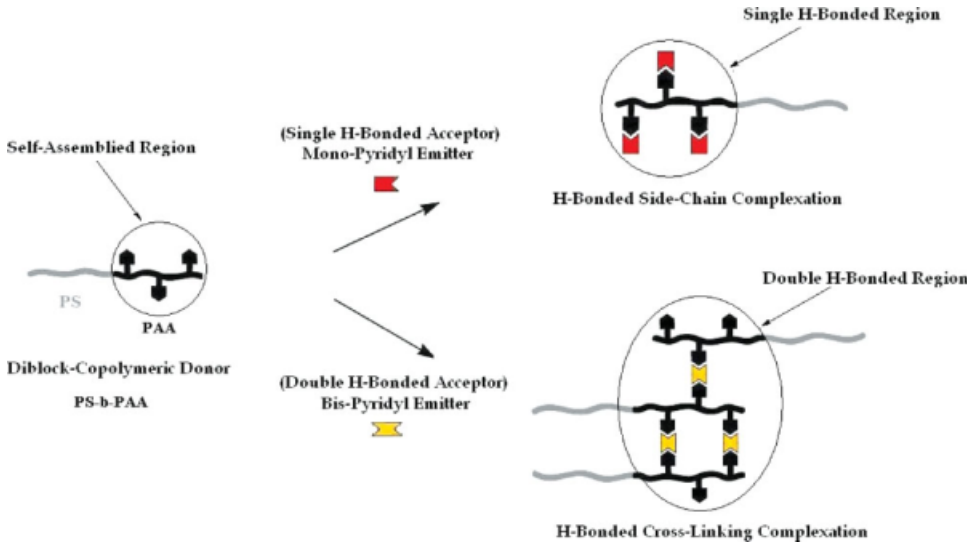

Figure 1. Schematic illustration of single (side-chain) and double (cross-linking) H-bonded complexes.

Cyclic voltammetry (CV) was performed at a scanning rate of 100 mV/s on a BAS 100 B/W electrochemical analyzer, which was equipped with a three-electrode cell. Pt wire was used as a counter electrode, and an Ag/AgCl electrode was used as a reference electrode in the CV measurements. The thin films of H-bonded complexes coated on Pt disk working electrode were anodically and cathodically scanned in an acetonitrile solution containing 0.1 M n-Bu_4NClO_4.[31]

Fabrication of PLED Devices

EL devices with the configuration of ITO/PEDOT:PSS (40–50 nm)/H-bonded complexes (50–60 nm)/BCP(10 nm)/Alq_3(30 nm)/LiF(1 nm)/Al(150 nm) were made, where BCP (i.e., 2,9-dimethyl-4,7-diphenyl-1,10-phenanthroline) or Alq_3 (i.e., tris(8-hydroxyquinoline)aluminium) was used as an electron transporting layer. The ITO substrates were routinely cleaned by ultrasonic treatments in detergent solutions and diluted water, followed by rinsing with acetone and then ethanol. After drying, the ITO substrates were kept in oxygen plasma for 4 min before being loaded into the vacuum chamber. The solutions (10 mg/mL) of light-emitting materials in chlorobenzene were spin-coated on glass slides precoated with indium tin oxide (ITO) having a sheet resistance of ~20 Ω/square and an effective individual device area of 3.14 mm^2. The spin coating rate was 6000 rpm for 60 s with PEDOT: PPS, 4000 rpm for 60 s with resulting polymers, and the thicknesses of PEDOT: PPS and H-bonded polymers were measured by an Alfa Step 500 Surface Profiler (Tencor). BCP and Alq_3 layers were thermally deposited at a rate of 1–2 Å/s under a pressure of $\sim 2 \times 10^{-5}$ torr in an Ulvac Cryogenic deposition system. Under the same deposition systems and conditions, one layer of LiF was thermally deposited as a cathode at a rate of 0.1–0.2 Å/s, which was followed by capping with an aluminum layer. The *I-V* characteristics in the dark and under illumination were measured with Keithley 236 source meter.

Syntheses of Diblock Copolymers P1-P3 and Hydrolysis of Diblock Copolymers PD1-PD3

A series of diblock copolymers **P1–P3**, that is, polystyrene-*block*-poly(*tert*-butyl acrylate)s **(PS-*b*-P*t*BuA)s**, were synthesized via anionic block copolymerization[32] using styrene and tBuA as monomers. Similar procedures for the syntheses of diblock copolymers **PD1–PD3**, that is, polystyrene-*block*-poly(acrylic acid)s **(PS-*b*-PAA)s**, were followed. Synthesis and characterization of diblock copolymers **P1–P3** and their hydrolysis of diblock copolymers **PD1–PD3** are described in the supporting information. The thermal properties and molecular weight characterization of the resulting copolymers **P1–P3**, that is, **(PS-*b*-P*t*BuA)s** with different molar ratios of styrene and tBuA (10/1, 5/1, and 2/1, i.e., the content of tBuA component was consecutively increased), are summarized in Table 1.

Table 1. Thermal Properties and Molecular Weights of Diblock-Copolymers (**P1**–**P3** and **PD1**–**PD3**)

Diblock Copolymer	Molar Ratio of Monomers (Styrene/tBuA)[a]	T_g[b] (° C)	T_d[c] (° C)	M_n[d] (g/mol)	PDI
PS_{328}-*b*-P*t*BuA_{33} (P1)	10/1	92	254,437	38,464	1.28
PS_{304}-*b*-P*t*BuA_{61} (P2)	5/1	95	237,391	39,468	1.33
PS_{210}-*b*-P*t*BuA_{105} (P3)	2/1	98	215,379	35,465	1.38
PS_{328}-*b*-PAA_{33} (PD1)	10/1	90	198,348	–	–
PS_{304}-*b*-PAA_{61} (PD2)	5/1	92	183,435	–	–
PS_{210}-*b*-PAA_{105} (PD3)	2/1	96	175,402	–	–

[a] Determined by ^{1}H-NMR spectra and the data of **PD1–PD3** followed the data of **P1–P3** due to **PAA** block obtained from the direct hydrolysis of block **P*t*BuA**.
[b] T_g values were determined by DSC at a heating rate of 10 °C/min under nitrogen.
[c] Degradation temperatures corresponding to P*t*BuA and PS blocks of diblock copolymers were determined by TGA at a heating rate of 10 °C/min under nitrogen.
[d] The number-average molecular weights were measured by GPC in THF using polystyrene standards.

Syntheses of Pyridyl Moieties as Proton Acceptors (Compounds 14–19)

1,4-Bi-octyloxybenzene (1)

Hydroquinoline (22.80 g, 0.207 mol), 1-bromoctane (100.00 g, 0.518 mol), and potassium hydroxide (35 g) were dissolved in the mixture of ethanol (675 mL) and water (75 mL), and heated to 80 °C for 48 h. After the reaction was completed, the solvent was removed by rotary evaporation, and the resulting mixture was extracted with dichloromethane and water for three times. The organic layer was collected and dried with anhydrous $MgSO_4$. After filtration and concentration, the product was purified by recrystallization from toluene and washed by hexane to obtain compound **1**.

Yield: 35%, ^{1}H NMR (ppm, $CDCl_3$): δ 0.88 (t, 6H), 1.28–1.43 (m, 20H), 1.70–1.79 (m, 4H), 3.89 (t, 4H, $J = 6.6$ Hz), 6.81(s, 4H).

1,4-Dibromo-2,5-bi-octyloxybenzene (2)

Compound **1** (30.78 g, 92.01 mmol) and carbon tetrachloride (50 mL) were mixed and stirred in a flask. Bromine (9.68 mL, 193.21 mmol) was added dropwise into the solution and heated to 70 °C overnight. After cooling, saturated aqueous $Na_2S_2O_3$ (200 mL) was poured into the solution to quench the excessive bromine, and the resulting mixture was extracted with CCl_4. The organic layer was dried over $MgSO_4$, and then the solvent was removed by rotary evaporation. The product was purified by recrystallization from hexane to isolate compound **2**. Yield: 86%, ^{1}H NMR (ppm, $CDCl_3$): δ 0.90 (t, 6H), 1.30–1.47 (m, 20H), 1.77–1.82 (m, 4H), 3.94 (t, 4H, $J = 6.6$ Hz), 7.08 (s, 2H).

4-Bromo-2,5-bi-octyloxybenzaldehyde (3)

Compound **2** (15 g, 30.24 mmol) was dissolved in anhydrous THF and cooled to −78 °C under nitrogen atmosphere. *n*-Butyl lithium (2.5 M in hexane, 14.5 mL, 36.68 mmol) was injected into the solution by means of a syringe. After reaction, the solution was stirred at −78 °C for 30 min, and then the reaction temperature was increased to −30 °C. DMF (3.51 mL, 45.35 mmol) was then added into the reaction mixture and stirred for 1.5 hr. After then, the solution was stirred at room temperature overnight. The resulting mixture was extracted with ethyl ether and water. The organic layer was collected and dried over anhydrous $MgSO_4$. After filtration and concentration, the product was purified by column chromatography using dichloromethane/hexane (1:40) as an eluant to give a yellow solid.

Yield: 70%, ^{1}H NMR (ppm, $CDCl_3$): δ 0.89 (t, 6H), 1.29–1.56 (m, 20H), 1.79–1.84 (m, 4H), 4.00 (t, 4H, $J = 6.6$ Hz), 7.22 (s, 1H), 7.31 (s, 1H), 10.41 (s, 1H).

2,5-Bi-octyloxy-4-(2-pyridin-4-yl-vinyl)benzaldehyde (4)

To a solution of compound **3** (6 g,13.63 mmol), palladium (II) acetate (0.122 g, 0.55 mmol), and tri-*o*-tolylphosphine (0.25 g, 0.81 mmol) in a mixture of benzene (20 mL) and triehtylamine (20 mL),

4-vinylpyridine (1.62 mL, 15.5 mmol) was added. The solution was heated to react at 120 °C for 48 hr. The resulting mixture was extracted with dichloromethane and water. The organic layer was collected and dried over anhydrous $MgSO_4$, and then the solvent was removed by rotary evaporation. The product was isolated through column chromatography (ethyl acetate/hexane, 1:10) as an eluant to give a yellow solid.

Yield: 40%, ^{1}H NMR (ppm, $CDCl_3$): δ 0.88 (t, 6H), 1.29–1.51 (m, 20H), 1.79–1.84 (m, 4H), 4.06 (t, 2H, J = 6.6 Hz), 4.11 (t, 2H, J = 6.6 Hz), 7.13–7.19 (d, 1H, J = 16.5 Hz), 7.17 (s, 1H), 7.34 (s, 1H), 7.38–7.40 (d, 2H, J = 6.0 Hz), 7.63–7.68 (d, 1H, J = 16.5 Hz), 8.60–8.62 (d, 2H, J = 6.0 Hz), 10.47 (s, 1H).

Benzyl-diethyl Phosphonate (5)

Benzyl bromide (5 g, 29.41 mmol) and triethyl phosphate (33 mL) were placed into a flask and stirred. The reaction was heated to react at 120 °C for 12 hr. After cooling, the excessive triethyl phosphate was removed by reduced pressure distillation, and then the residue was dried *in vacuo* to get the desired product.

Yield: 90%, ^{1}H NMR (ppm, $CDCl_3$): δ 1.22–1.27 (t, 6H), 3.05 (d, 4H, J = 21.3 Hz), 4.00–4.05 (m, 4H), 7.22–7.31 (m, 5H).

4-Cyanobenzyl Diethyl Phosphonate (6)

Compound **6** was obtained from the starting material of alpha-bromo-*p*-tolunitrile, following a similar procedure as described for compound **5**.

Yield: 88%, ^{1}H NMR (ppm, $CDCl_3$): δ 1.24–1.31 (t, 6H), 3.17 (d, 4H, J = 22.2 Hz), 4.02–4.11 (m, 4H), 7.41 (d, 2H, J = 8.0 Hz), 7.62 (d, 2H, J = 7.8 Hz).

4-Methylbenzoic Acid N′-Benzoylhydrazide (7)

Appropriate amount of benzoyl chloride in anhydrous chloroform was added dropwise into a solution of *p*-toluic hydrazide (3 g, 19.78 mmol) in a mixture of dry chloroform and triethylamine under nitrogen atmosphere. The reaction was stirred at room temperature for 1.5 h. The resulting mixture was collected by filtration and washed with water and hexane. The residue was dried *in vacuo* to obtain the product.

Yield: 84%, ^{1}H NMR (ppm, $CDCl_3$): δ 2.49 (s, 3H), 7.42 (d, 2H, J = 8.1 Hz), 7.60–7.73 (m, 3H), 7.95 (d, 2H, J = 8.7 Hz), 8.02 (d, 2H), 10.55 (d, 2H, J = 11.7 Hz).

2-Phenyl-5-p-tolyl-[1,3,4]oxadiazole (8)

A solution of compound **7** (1.5 g, 5.9 mmol) in $POCl_3$ (40 mL) was stirred under nitrogen atmosphere, and heated to 110 °C for 6 h. After cooling, the solvent was removed by reduced pressure distillation and a brown viscous liquid was acquired. A precipitate was collected by pouring water into the resulting mixture. A white needle solid was obtained by filtration and recrystallization from methanol.

Yield: 70%, ^{1}H NMR (ppm, $CDCl_3$): δ 2.42 (s, 3H), 7.31 (d, 2H, J = 7.8 Hz), 7.51 (m, 3H), 7.95 (d, 2H, J = 8.7 Hz), 8.02 (d, 2H, J = 8.2 Hz), 8.13 (d, 2H, J = 7.8 Hz).

2-(4-Bromomethyl-phenyl)-5-phenyl-[1,3,4]oxadiazole (9)

Compound **8** (3.00 g, 12.70 mmol), *N*-bromosuccinimide (2.4 g, 13.90 mmol), and benzoyl peroxide (0.3 g, 0.127 mmol) were dissolved in carbon tetrachloride (80 mL). The reaction mixture was heated to react at 85 °C for 5 h. After the reaction was completed, the product in solution was collected by filtration and purified by recrystallization from a solution of chloroform/methanol (4:1) to give a white solid.

Yield: 60%, ^{1}H NMR (ppm, $CDCl_3$): δ 2.42 (s, 3H), 7.31 (d, 2H, J = 7.8 Hz), 7.50 (m, 3H), 8.11 (d, 2H, J = 7.8 Hz), 8.13 (m, 2H).

[4-(5-Phenyl-[1,3,4]oxadiazol-2-yl)-benzyl] Diethyl Phosphonate (10)

Compound **10** was synthesized using compound **9** as a staring material and followed by a similar synthetic procedure of compound **5**.

Yield: 90%, ^{1}H NMR (ppm, $CDCl_3$): δ 1.18–1.29 (t, 6H), 3.20 (d, 2H, J = 22.1 Hz), 4.02–4.10 (m, 4H), 6.82 (d, 2H, J = 8.7 Hz), 6.89 (d, 3H), 7.17 (d, 2H, J = 8.7 Hz), 7.21 (m, 2H).

1-Methyl-4-octyloxybenzene (11)

To a solution of *p*-cresol (20 g, 0.19 mol) and potassium hydroxide (15.5 g, 0.277 mol) in a mixture of water (15 mL) and ethanol (135 mL), 1-bromooctane (42.86 g, 0.22 mol) was added. The mixture was heated to reflux for 24 h. As the reaction was completed, the solvent was removed by rotary evaporation and the resulting mixture was extracted with dichloromethane and water. The organic layer was collected and dried with

anhydrous $MgSO_4$. After filtration and concentration, the product was purified by a silica gel column using hexane/ethyl acetate (50:1 then 1:1) as an eluent to obtain a brown viscous liquid.

Yield: 88%, ^{1}H NMR (ppm, $CDCl_3$): δ 0.88 (t, 3H, J = 6.3 Hz), 1.28–1.52 (m, 10H), 1.69–1.79 (m, 4H), 2.26 (s, 3H), 3.88 (d, 2H, J = 6.4 Hz), 6.77 (d, 2H, J = 8.6 Hz), 7.05 (d, 2H, J = 8.6 Hz).

(4-Octyloxybenzyl)-Triphenylphosphonium Bromide (12)

Compound **11** (15.00 g, 0.068 mol), *N*-bromosuccinimide (14.53 g, 0.082 mol), and AIBN (1.34 g, 0.008 mol) were dissolved in carbon tetrachloride (100 mL). The reaction mixture was heated to react at 70 °C for 4 h. After cooling, the excessive NBS and AIBN were removed by filtration and the solution was concentrated by rotary evaporation to give a brown viscous liquid product *p*-octyloxybenzyl bromide (Yield: 90 %). Because of the unstability of this bromide compound, the subsequent procedure continued immediately as follows: The bromide compound (15.00 g, 0.054 mol) and triphenyl phosphate (15.50 g, 0.059 mol) were dissolved in xylene (200 mL). The reaction mixture was heated to react at 110 °C for 18 h. After completion of the reaction, the product in solution was collected by filtration and washed with hexane to remove the excessive triphenyl phosphate, and then it was dried *in vacuo* to acquire compound **12**.

Yield: 88%, ^{1}H NMR (ppm, $CDCl_3$): δ 0.88 (t, 3H, J = 6.3 Hz), 1.18–1.22 (m, 18H), 1.70–1.75 (m, 4H), 3.92 (t, 2H, J = 6.4 Hz), 5.22 (d, 2H, J = 20.2 Hz), 6.70 (d, 2H, J = 8.4 Hz), 6.92 (d, 2H, J = 8.4 Hz), 7.45–7.82 (m, 15H).

(Triphenylphosphonium bromide)-Thiophene (13)

Compound **13** was synthesized from a starting material of 2-methylthiophene, and followed by a similar procedure as described for compound **12**.

Yield: 78%, ^{1}H NMR (ppm, $CDCl_3$): δ 5.75 (d, 2H, J = 13.2 Hz), 6.86 (m, 1H), 7.07 (m, 1H), 7.07(m, 1H), 7.62–7.82 (m, 15H, J = 6.4 Hz).

General Procedure of Horner-Wadsworth-Emmons Reaction for Proton Acceptors (Compounds 14–18)

Compound **4** (0.8 g, 71 mmol) and compound **5** (0.51 g, 2.24 mmol) were placed in a flask. A solution of anhydrous THF (50 mL) and chloroform (50 mL) was injected under nitrogen atmosphere by means of a syringe and heated to 80 °C. Sodium hydride (0.12 g, 5.13 mmol) in anhydrous THF (10 mL) was slowly injected into the solution and reacted at room temperature for 20 h. The resulting mixture was extracted with dichloromethane and water. The organic layer was collected and dried with anhydrous $MgSO_4$. After filtration and concentration, the product was purified by an Al_2O_3 column using hexane/ethyl acetate (10:1) as an eluent to obtain compound **14**. The syntheses of compounds **15**, **16**, **17**, and **18** were also followed by the similar procedure.

trans,trans-4-[2-(2,5-Bi-octyloxy-4-styryl-phenyl)-vinyl]-pyridine (14)

Yield: 78%, ^{1}H NMR (ppm, $CDCl_3$): δ 0.88 (t, 6H), 1.29–1.51 (m, 20H), 1.86–1.90 (m, 4H), 4.03–4.10 (m, 4H), 7.02–7.08 (d, 1H, J = 16.5 Hz), 7.12 (s, 1H), 7.14 (s, 1H), 7.19 (d, 1H, J = 16.5 Hz), 7.26 (m, 1H), 7.29–7.34 (d, 1H, J = 16.5 Hz), 7.34–7.39 (m, 4H), 7.45–7.51 (d, 1H, J = 16.5 Hz), 7.53–7.55 (d, 2H, J = 5.2 Hz), 8.56–8.57 (d, 2H, J = 5.1 Hz); ^{13}C NMR (ppm, $CDCl_3$): δ 14.10, 22.66, 26.27, 29.39, 31.80, 69.42, 69.58, 110.12, 111.02, 120.79, 123.24, 125.33, 125.82, 126.56, 127.58, 128.20, 128.64, 129.48, 137.72, 145.30, 150.07, 150.96, 151.51; Found: C, 82.22; H, 9.05; N, 2.21%. Calcd. for $C_{37}H_{49}NO_2$: C, 82.23; H, 9.15; N, 2.59 %.

trans,trans-4-{2-[2,5-Bi-octyloxy-4-(2-pyridin-4-yl-vinyl)-phenyl]-vinyl}-benzonitrile (15)

Yield: 72%, ^{1}H NMR (ppm, $CDCl_3$): δ 0.88 (t, 6H), 1.25–1.58 (m, 20H), 1.85–1.93 (m, 4H), 4.07 (m, 4H), 7.05–7.10 (d, 1H, J = 16.5 Hz), 7.12–7.17 (d, 1H, J = 16.5 Hz), 7.11 (s, 2H), 7.36–7.38 (d, 2H, J = 5.7 Hz), 7.55–7.65 (m, 4H), 7.57–7.52 (d, 1H, J = 16.5 Hz), 7.64–7.69 (d, 1H, J = 16.5 Hz), 8.56–8.58 (d, 2H, J = 4.8 Hz); ^{13}C NMR (ppm, $CDCl_3$): δ 14.08, 22.64, 26.24, 29.27, 29.35, 31.77, 69.45, 110.74, 110.85, 119.92, 120.82, 126.83, 127.04, 127.36, 127.81, 132.44, 142.32, 145.24, 150.13, 151.31, 151.38; Found: C, 80.58; H, 8.12; N, 4.60%. Calcd. for $C_{38}H_{48}N_2O_2$: C, 80.81; H, 8.57; N, 4.96 %.

trans,trans-4-(2-{2,5-Bi-octyloxy-4-[2-(4-octyloxy-phenyl)-vinyl]-phenyl}-vinyl)-pyridine (16)

Yield: 72%, ^{1}H NMR (ppm, $CDCl_3$): δ 0.88 (t, 6H), 0.96 (t, 3H), 1.29–1.54 (m, 30H), 1.74–1.89 (m, 6H), 3.99 (t, 2H, J = 6.3 Hz), 4.07 (m, 4H), 6.88 (s, 1H), 6.91 (s, 1H), 7.01–7.06 (d, 1H, J = 16.5 Hz),

7.08–7.13 (d, 1H, J = 16.5 Hz), 7.10–7.11 (d, 2H, J = 4.8 Hz), 7.30–7.36 (d, 1H, J =1 6.5 Hz), 7.37 (d, 2H, J = 4.5 Hz), 7.44–7.47 (d, 2H, J = 4.8 Hz), 7.64–7.69 (d, 1H, J = 16.5 Hz), 8.54–8.56 (d, 2H, J = 6.0 Hz); ^{13}C NMR (ppm, $CDCl_3$): δ 14.07, 22.24, 26.01, 26.26, 28.87, 29.45, 29.39, 31.78, 68.03, 69.37, 69.57, 110.12, 111.02, 114.65, 123.91, 124.76, 125.46, 127.76, 128.18, 128.70, 129.15, 130.30, 145.44, 149.95, 150.74, 151.55, 158.91; Found: C, 80.49; H, 9.75; N, 2.19%. Calcd. for $C_{45}H_{65}NO_3$: C, 80.91; H, 9.81; N, 2.10 %.

trans,trans-4-[2-(2,5-Bi-octyloxy-4-{2-[4-(5-phenyl-[1,3,4]oxadiazol-2-yl)-phenyl]-vinyl}-phenyl)-vinyl]-pyridine (17)

Yield: 73%, ^{1}H NMR (ppm, $CDCl_3$): δ 0.89 (t, 6H), 1.25–1.59 (m, 20H), 1.88–1.92 (m, 4H), 4.10 (m, 4H), 7.05–7.10 (d, 1H, J = 16.5 Hz), 7.13 (s, 1H), 7.15 (s, 1H), 7.19–7.24 (d, 1H, J = 16.5 Hz), 7.37–7.39 (d, 2H, J = 6.0 Hz), 7.53–7.58 (d, 1H, J = 15.9 Hz), 7.54–7.70 (m, 5H), 7.65–7.70 (d, 1H, J = 16.5 Hz), 8.09–8.17 (m, 4H), 8.56–8.58 (d, 2H, J = 4.8 Hz); ^{13}C NMR (ppm, $CDCl_3$): δ 14.09, 22.66, 26.26, 29.29, 31.80, 69.41, 110.58, 110.92, 120.80, 126.23, 126.87, 127.00, 127.22, 127.35, 127.91, 128.09, 129.04, 131.67, 141.17, 145.16, 150.07, 151.20, 151.44, 164.42; Found: C, 78.99; H, 7.52; N, 5.92%. Calcd. for $C_{45}H_{53}N_3O_3$: C, 79.03; H, 7.81; N, 6.14 %.

trans,trans-4-{2-[2,5-Bi-octyloxy-4-(2-thiophene-2-yl-vinyl)-phenyl]-vinyl}-pyridine (18)

Yield: 62%, ^{1}H NMR (ppm, $CDCl_3$): δ 0.88 (t, 6H), 1.30–1.60 (m, 20H), 1.85–1.90 (m, 4H), 4.06 (m, 4H), 7.01–7.06 (d, 1H, J = 16.8 Hz), 7.02–7.07 (d, 1H, J = 16.0 Hz), 7.01–7.10 (m, 2H), 7.20–7.22 (d, 1H), 7.27 (s, 2H), 7.35–7.37 (d, 1H, J = 15.5 Hz), 7.35–7.37 (d, 2H, J = 6.0 Hz), 7.63–7.69 (d, 1H, J = 16.5 Hz), 8.55–8.57 (d, 2H, J = 6.0 Hz); ^{13}C NMR (ppm, $CDCl_3$): δ 14.10, 22.67, 26.26, 29.29, 29.39, 29.44, 31.80, 69.38, 69.56, 110.46, 111.01, 120.77, 122.80, 123.13, 124.43, 125.23, 125.81, 127.60–127.77, 128.01, 143.58, 145.29, 150.06, 150.91, 151.47; Found: C, 76.53; H,8.91; N, 2.02%. Calcd. for $C_{35}H_{47}NO_2S$: C, 77.02; H, 8.68; N, 2.57 %.

trans,trans-2,5-Dioctyloxy-1,4-bis(2-[4]pyridyl-ethenyl)benzene (19)

Compound **19** was synthesized by Heck reaction and followed by the similar method described for compound **4**.

Yield: 20%, ^{1}H NMR (ppm, $CDCl_3$): δ 0.88 (t, 6H), 1.26–1.62 (m, 20H), 1.80–1.92 (m, 4H), 4.07 (t, 4H, J = 6.6 Hz), 7.10 (d, 2H, J = 16.0 Hz), 7.13 (s, 2H), 7.43 (d, 4H, J = 5.7 Hz), 7.79 (d, 2H, J = 16.5 Hz), 8.58 (d, 4H, J = 5.1 Hz); ^{13}C NMR (ppm, $CDCl_3$): δ 14.08, 22.65, 26.27, 29.29, 29.38, 29.41, 31.80, 9.52, 110.99, 120.82, 126.65, 126.72, 127.86, 145.08, 150.17; Found: C, 79.27; H,8.67; N, 5.16%. Calcd. for $C_{36}H_{48}N_2O_2$: C, 79.96; H, 8.95; N, 5.18 %.

RESULTS AND DISCUSSION

Herein, supramolecular H-bonded complexes containing photoluminescent pyridyl compounds **PBB-OC$_8$ (14), PBBCN-OC$_8$ (15), PBBOC$_8$-OC$_8$ (16), PBBOXD-OC$_8$ (17), PBT-OC$_8$ (18)**, and **PBP-OC$_8$ (19)** as proton acceptors and amphiphilic diblock copolymers **PS$_{328}$-*b*-PAA$_{33}$ (PD1), PS$_{304}$-*b*-PAA$_{61}$ (PD2)**, and **PS$_{210}$-*b*-PAA$_{105}$ (PD3)** with side-chain carboxylic acid groups contributed from PAA segments as proton donors were prepared and studied. The synthetic routes of block copolymers **(PS-*b*-PAA)s** (i.e., **PD1-PD3**), which were hydrolyzed from **(PS-*b*-P*t*BuA)s** (i.e., **P1-P3**), and pyridyl compounds **14–19** are outlined in Schemes 1 and 2. Mono-pyridyl (single H-bonded) proton acceptors **PBB-OC$_8$ (14)**, **PBBCN-OC$_8$ (15)**, **PBBOC$_8$-OC$_8$ (16)**, **PBBOXD-OC$_8$ (17)**, and **PBT-OC$_8$ (18)** were synthesized via the efficient Horner-Wadsworth-Emmons reactions, which were conducted for the linkages of carbon-carbon double bonds among conjugated cores, to connect the intermediate product **4** with the structural units of benzene, cyano benzene, octoxy benzene, oxadiazole, and thiophene. The Heck reaction was used for the synthesis of bis-pyridyl (double H-bonded) proton acceptor **PBP-OC$_8$ (19)**. The details of synthetic procedures for these H-bonded acceptors **14–19** were described in the experimental section.

Syntheses and Characterization of Diblock Copolymers P1-P3 and PD1-PD3

The syntheses of diblock copolymers **(PS-*b*-P*t*BuA)s** (i.e., **P1–P3**) were carried out by anionic copolymerization. Copolymers **(PS-*b*-P*t*BuA)s** with different monomer compositions were prepared using the following feed-in molar ratios of styrene/tBuA = 10/1, 5/1, and 2/1, correspondingly. The structural compositions of styrene and tBuA constituents in the copolymers were identified by ^{1}H NMR spectra, where the molar ratios of

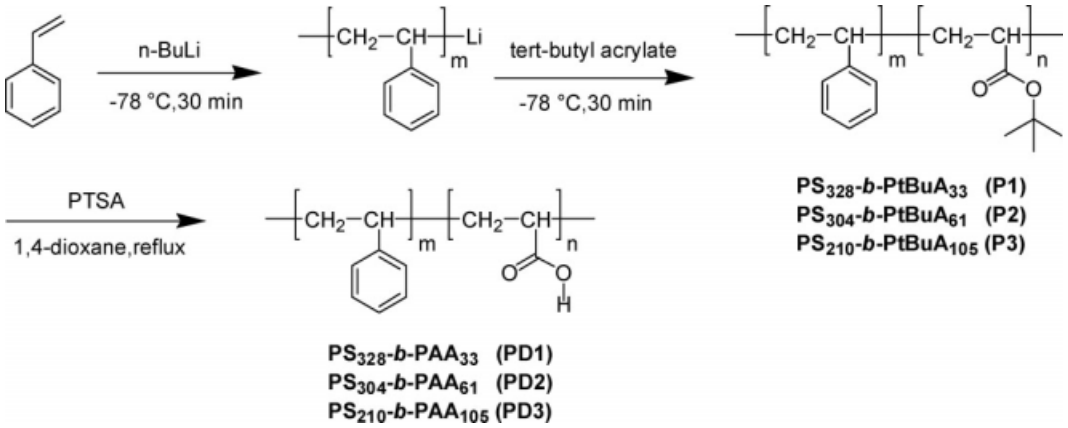

Scheme 1. Synthetic routes of diblock copolymers as proton donors.

PS and P*t*BuA blocks were estimated from the integrated values of proton peaks in phenyl rings (two broad characteristic peaks at 6.8–7.6 ppm) attributed from PS blocks as well as those in —C(CH_3)$_3$ (a peak at 1.58 ppm) from P*t*BuA blocks. The NMR results closely match with those expected on the basis of feed-in molar ratios of monomers used in anioinic copolymerization for diblock copolymers (see Table 1). The structures of copolymers were also confirmed by FTIR analyses of absorption bands at 3026 cm^{-1} (aromatic Ar—H stretching), 2978 cm^{-1} (*tert*-butyl C—H stretching), 2850–2950 cm^{-1} (backbone C—H stretching), 1729 cm^{-1} (ester C=O stretching), and 1368 cm^{-1} (*tert*-butyl C–H bending) and the example of copolymer **P1** is shown in Figure 2(a). The molecular weights of the block copolymers **P1–P3** displayed in Table 1 were determined by gel permeation chromatography (GPC) using THF as the eluent and calibrated against polystyrene as standards. The number-average molecular weights (M_n) of block copolymers were in the range of 35,500–39,500 g/mol, and the polydispersity indexes were between 1.28 and 1.38. The molecular weights of **(PS-*b*-PAA)s** (i.e., **PD1–PD3**) were estimated from **(PS-*b*-P*t*BuA)s** (i.e., **P1–P3**) before hydrolysis, because **PD1–PD3** can not be measured by GPC due to the strong polarity of acid groups from PAA blocks. The thermal properties of these copolymers in nitrogen were detected by thermogravimetric analysis (TGA) and differential scanning calorimetry (DSC). As shown in Table 1, all copolymers demonstrate similar TGA results with two principal degradation temperatures (T_d) corresponding to P*t*BuA (with a lower T_d) and PS blocks (with a higher T_d), respectively. The copolymer **PS_{328}-*b*-P*t*BuA_{33} (P1)** (90.9 mol% of PS content) reveals the highest (two-step) T_d values at 254 and 437 °C. The thermal stability of PS blocks containing benzene structures is greater than that of hydrocarbon-based P*t*BuA blocks, which leads the decreased *T*d values of copolymers when the PS content reduces from 90.9 to 66.7 mol %, that is, *T*d: **P3** < **P2** < **P1**. However, **PS_{210}-*b*-P*t*BuA_{105} (P3)** exhibits the highest glass transition temperature (T_g) at 98 °C, so the enhanced T_g value of the copolymer with the higher P*t*BuA content might be attributed to the stronger interaction of polar tBuA moieties.

Hydrolyses of Diblock Copolymers

The tBuA segments of diblock copolymers **(PS-*b*-P*t*BuA)s** (i.e., **P1–P3**) were hydrolyzed by a previously described procedure (as shown in the experimental section). Under this hydrolysis reaction, *p*-toluenesulphonic acid in 1,4-dioxane was used as a hydrolyzing agent to selectively cleave the *tert*-butyl ester groups, and then the acrylic acid groups were hydrolyzed to yield amphiphilic block copolymers **(PS-*b*-PAA)s** (i.e., **PD1–PD3**). Both ^{1}H NMR and FTIR spectra were used to monitor the recovery of acid functionality. The disappearance of ^{1}H NMR peak at 1.58 ppm indicates the hydrolysis of *tert*-butyl ester groups to become acid groups. As shown in Figure 2(b), the alteration in absorption bands of FTIR spectrum in **PS_{328}-*b*-PAA_{33} (PD1)** associated with a broaden peak at 1736 cm^{-1} (carboxylic acid C=O stretching) and the disappearance of the *tert*-butyl group at 1368 cm^{-1} (*tert*-butyl C—H bending) were also applied to confirm the complete transformation of ester to carboxylic groups. The thermal properties of these hydrolyzed copolymers **PD1–PD3** show two broad decomposition

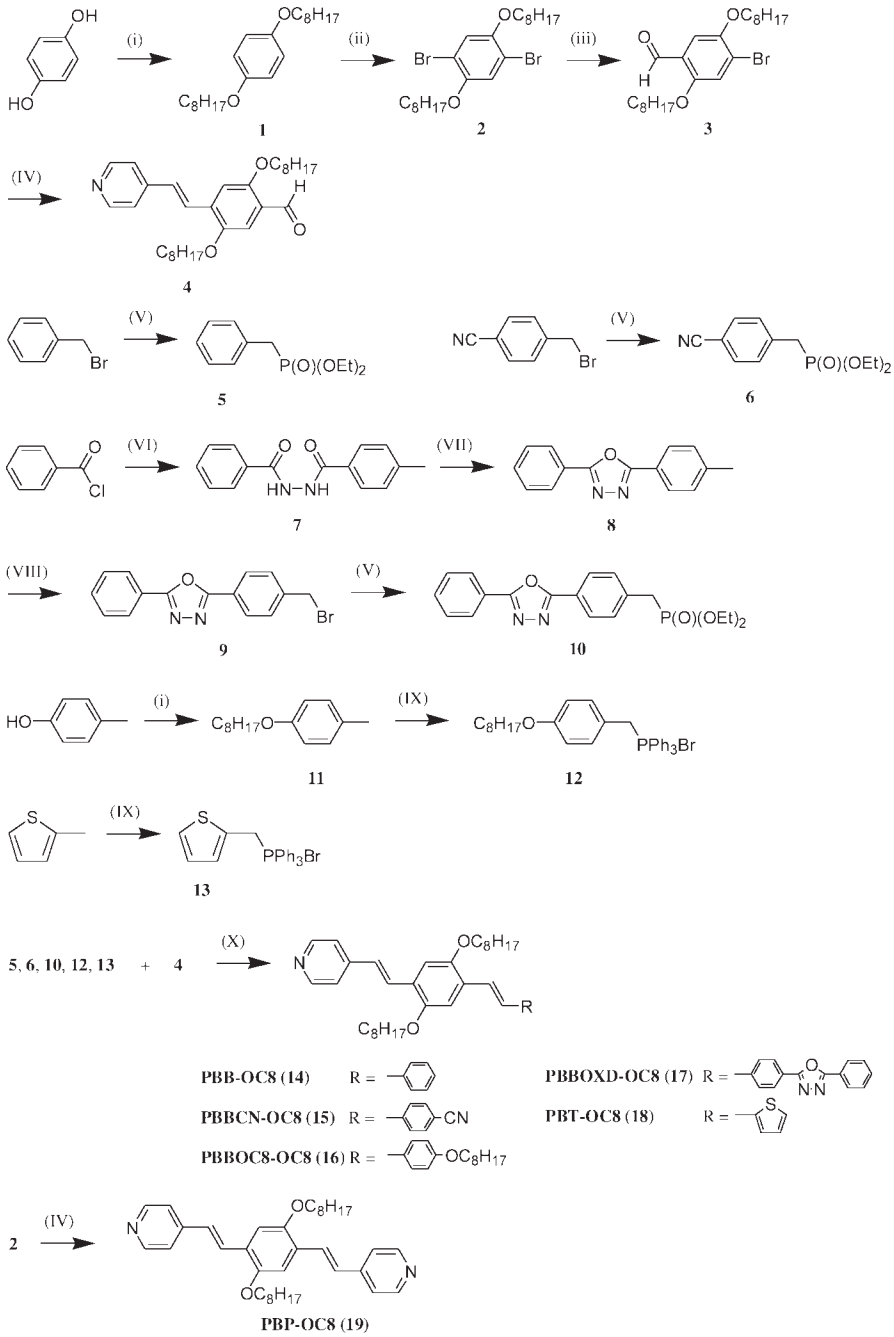

Reagent: (i) $C_8H_{17}Br$, KOH(*aq*)/EtOH; (ii) Br_2/CCl_4; (iii) n-BuLi, DMF, -78 °C; (IV) $Pd(OAc)_2$, tri-o-tolylphosphine, benzene/Et3N; (V) triethyl phosphate; (VI) *p*-toluic hydrazide, CH_3Cl/Et_3N; (VII) $POCl_3$; (VIII) benzoyl peroxide, NBS, CCl_4; (IX) 1. AIBN, NBS, CCl_4. 2. triphenyl phosphate; (X) NaH, $CHCl_3$/THF.

Scheme 2. Synthetic routes of pyridyl compounds as proton acceptors.

transitions in the range of 175–198 °C (PAA block) and 348–402 °C (PS block). As shown in Table 1, the T_g and T_d (first decomposition temperatures corresponding to PAA or P*t*BuA blocks) values of the resulting copolymers **PD1–PD3** containing PAA were lower than those of their analogous copolymers **P1–P3** (before hydrolyses), respectively. The lower T_d values (first decomposition

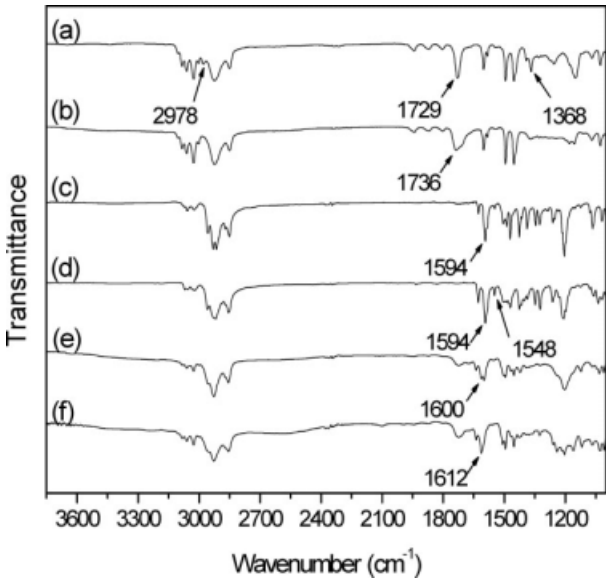

Figure 2. FTIR spectra of (a) **PS_{328}-*b*-P*t*BuA_{33}** (**P1**), (b) **PS_{328}-*b*-PAA_{33}** (**PD1**), (c) **PBB-OC_8 (14)**, (d) **PBP-OC_8** (**19**), (e) **PS_{328}-*b*-PAA_{33}/PBB-OC_8** (**PD1/14**), and (f) **PS_{328}-*b*-PAA_{33}/PBP-OC_8** (**PD1/19**).

temperatures) of **PD1-PD3** containing PAA than those of **P1–P3** (before hydrolyses) is because the PAA block has lower thermal stability than the P*t*BuA block in **P1–P3**, which is consistent with the reported literature.[33] The decreased T_d values of copolymers **P1–P3** were observed when the PS content reduces from 90.9 to 66.7 mol %, i.e., *T*d: **P1** > **P2** > **P3**. Similar to the trends of T_g and T_d values (first decomposition temperatures) in **P1–P3**, T_d values of copolymers decrease as the PS content reduces (i.e., T_d: **PD3** < **PD2** < **PD1**), and the enhanced T_g value of copolymer **PD3** (with the highest PAA content) among **PD1-PD3** might be due to the stronger interaction of polar AA moieties.

Characterization of H-Bonded Complexes

H-bonded complexes (all donor and acceptor moieties are fully H-bonded) formed by proton donor polymers **(PS-*b*-PAA)s** (i.e., **PD1–PD3**) with mono-pyridyl acceptors **14–18** and bis-pyridyl acceptor **19** (1:1 and 2:1 in molar ratios of donor:-acceptor to form H-bonded side-chain and cross-linking copolymers, respectively) were prepared by slow evaporation of solvents (THF) from their solutions (donors and acceptors were well dissolved), followed by drying in *vacuo* at 50 °C. As shown in Figure 2(c,d), a strong peak at 1594 cm^{-1} and a weak peak at 1548 cm^{-1} measured by FTIR experiments were assigned to the typical C=C and C=N vibrations of the free pyridyl units in compounds **PBB-OC_8 (14)** and **PBP-OC_8 (19)**. The shifts of the FTIR peaks from the free pyridyl units of 1594 and 1548 cm^{-1} in **PBB-OC_8 (14)** and **PBP-OC_8 (19)** to the H-bonded complexed pyridyl bands of 1600 and 1612 cm^{-1} in H-bonded complexes **PS_{328}-*b*-PAA_{33}/PBB-OC_8 (PD1/14)** and **PS_{328}-*b*-PAA_{33}/PBP-OC_8 (PD1/19)**, as shown in Figure 2(e,f), suggest the H-bonded interaction occurred between the pyridyl groups of **PBB-OC_8 (14)** and **PBP-OC_8 (19)** and the carboxylic acids of **PS_{328}-*b*-PAA_{33} (PD1)** in the H-bonded architectures.[34,35]

The melting temperatures (T_m) and decomposition temperatures (T_d) of proton acceptors **14–19** evaluated by DSC and TGA are shown in Table 2. Comparing the T_m values of all pyridyl acceptors, it demonstrates the higher T_m values of **PBBCN-OC_8 (15)** and **PBP-OC_8 (19)** resulted from the

Table 2. Thermal and Optical Properties of Proton Acceptors (**14–19**)

Compound	T_m[a] (°C)	T_d[b] (°C)	λ_{abs}[c] (nm)	$\lambda_{PL,soln}$[d] (nm)	$\lambda_{PL,film}$[e] (nm)
PBB-OC8 (14)	108	327	324,399	451	493
PBBCN-OC8 (15)	119	324	332,404	464	502
PBBOC8-OC8 (16)	73	376	399	456	498
PBBOXD-OC8 (17)	88	396	345,409	467	522
PBT-OC8 (18)	95	338	404	460	512,557
PBP-OC8 (19)	136	292	330,394	457	496

[a] Determined by DSC at a scanning rate of 10 °C/min.
[b] Five percent weight loss determined by TGA at a scanning rate of 10 °C/min.
[c] Wavelength of the maximum absorbance in spin-coated thin films.
[d] Wavelength of the maximum PL emission in dilute THF solutions.
[e] Wavelength of the maximum PL emission in solid state.

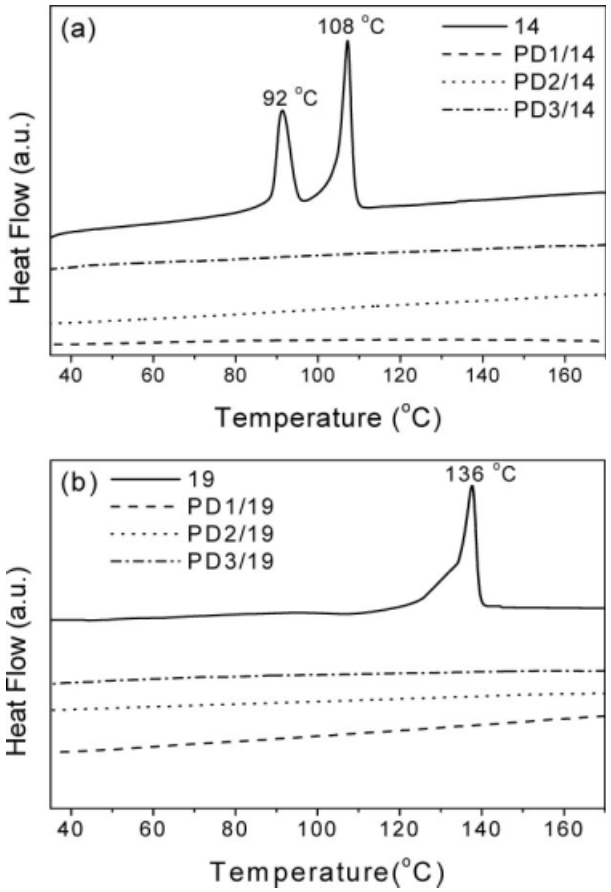

Figure 3. DSC curves of pyridyl compounds (a) **PBB-OC$_8$** (**14**), (b) **PBP-OC$_8$** (**19**), and their H-bonded complexes with **PS$_{328}$-*b*-PAA$_{33}$** (**PD1**), **PS$_{304}$-*b*-PAA$_{61}$** (**PD2**), and **PS$_{210}$-*b*-PAA$_{105}$** (**PD3**), respectively.

high polarities of cyano- and bis-pyridyl moieties. Compound **PBBOC$_8$-OC$_8$ (16)** displays the lowest T_m value at 73 °C corresponding to the flexible alkoxy terminal of -OC$_8$. However, no thermal transition peaks corresponding to T_m of pyridyl acceptors and T_g of donor copolymers **PD1-PD3** were not observed after the formation of H-bonded supramolecular architectures (Fig. 3), which indicates these components are completely miscible (without phase separation) in solid state of H-bonded complexes. As described previously, two distinct decomposition temperatures of pure copolymers **PS$_{328}$-*b*-PAA$_{33}$ (PD1)** (T_d = 198 and 348 °C) and **PS$_{210}$-*b*-PAA$_{105}$ (PD3)** (T_d = 175 and 402 °C) were found in TGA analyses, whereas H-bonded complexes **PS$_{328}$-*b*-PAA$_{33}$/PBBOC$_8$-OC$_8$ (PD1/16)** and **PS$_{328}$-*b*-PAA$_{33}$/PBP-OC$_8$ (PD1/19)** did not display two distinct decomposition temperatures in Figure 4(a). Similar decomposition behavior in H-bonded complexes **PS$_{210}$-*b*-PAA$_{105}$/PBBOC$_8$-OC$_8$ (PD3/16)** and **PS$_{210}$-*b*-PAA$_{105}$/PBP-OC$_8$ (PD3/19)** were also observed in Figure 4(b). Moreover, compared with the lower decomposition temperatures of PAA blocks in **PD1** and **PD3** (175 and 198 °C, respectively), the higher decomposition temperatures of PAA blocks in corresponding H-bonded complexes (T_d = 224, 218, 256, 231 °C for **PD1/16**, **PD1/19**, **PD3/16**, and **PD3/19**, respectively) were attributed to the H-bonded donor and acceptor interactions in the supramolecular architectures.

Optical Properties

UV-vis absorption and PL spectral data of the conjugated pyridyl compounds **14–19** are summarized in Table 2 and Figure 5. Most spectra exhibit two major absorption peaks around 330 and 400 nm in solid state. Upon excitation by the incident beam of 398 nm for the pyridyl compounds, the emission spectra of solid films display $\lambda_{max,PL}$

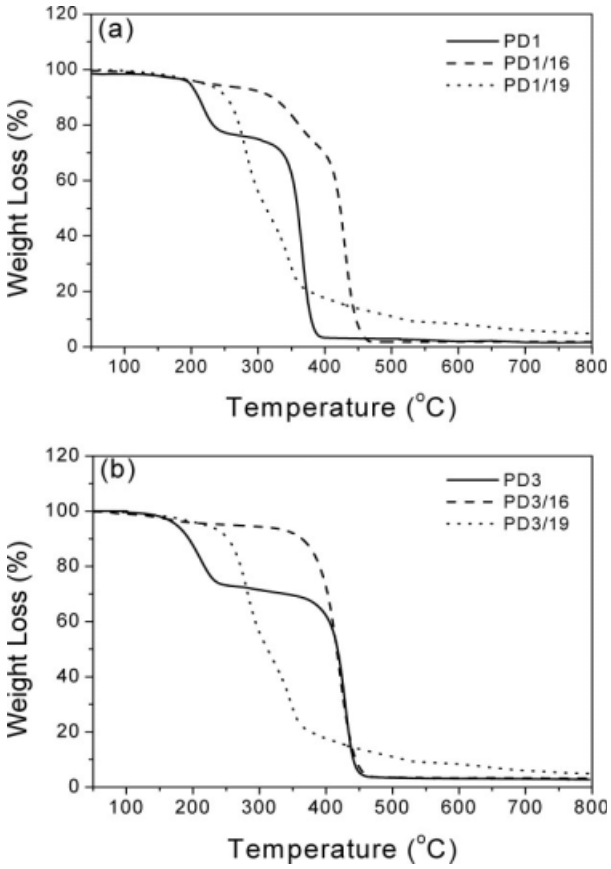

Figure 4. Comparison of TGA curves of (a) **PS$_{328}$-*b*-PAA$_{33}$** (**PD1**), (b) **PS$_{210}$-*b*-PAA$_{105}$** (**PD3**), and their H-bonded complexes with mon-pyridyl **PBBOC$_8$-OC$_8$** (**16**) and bis-pyridyl **PBP-OC$_8$** (**19**), respectively.

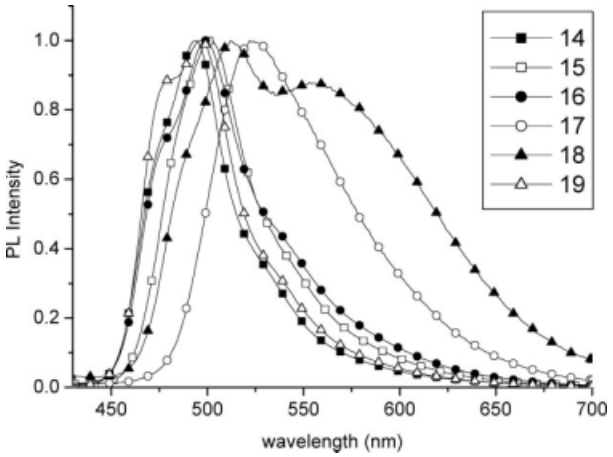

Figure 5. PL spectra of conjugated pyridyl compounds **PBB-OC$_8$** (**14**), **PBBCN-OC$_8$** (**15**), **PBBOC$_8$-OC$_8$** (**16**), **PBBOXD-OC$_8$** (**17**), **PBT-OC$_8$** (**18**), and **PBP-OC$_8$** (**19**) in solid films upon an excitation wavelength at 398 nm.

values between 493 and 557 nm in these compounds with various terminal structures. Monopyridyl compounds **PBBOXD-OC$_8$ (17)** and **PBT-OC$_8$ (18)** display the longest PL emission wavelengths ($\lambda_{PL,film}$ at 522 and 512/557 nm, respectively) among these light-emitting acceptors by virtue of the lower oxidation potentials and smaller energy gaps of the oxadiazole and thiophene moieties. According to our previous work,[18,28d] the H-bonded effects on photoluminescent pyridyl molecules in solid films have been surveyed to generate red shifts of the maximum emission peaks up to 100 nm depending on the nonphotoluminescent proton donors. In this study, the influence of H-bonds on pyridyl acceptors in their H-bonded supramolecular systems by diblock copolymeric donors were investigated, where the corresponding data are displayed in Table 3 and Figure 6. It is noticed H-bonded complexes show slightly red shifts of PL emissions

Table 3. Absorption and PL Emission Spectral Data of Proton Acceptors and Their H-Bonded Complexes (with Polymeric Donors) in Solid Films

Compounds or H-Bonded Complexes	λ_{abs}[a] (nm)	λ_{PL}[b] (nm)	$\Delta\lambda_{PL}$[c] (nm)
PBB-OC8 (14)	324,399	493	
PS$_{328}$-*b*-PAA$_{33}$/PBB-OC8 (PD1/14)	335,409	496	3
PS$_{304}$-*b*-PAA$_{61}$/PBB-OC8 (PD2/14)	322,419	585	92
PS$_{210}$-*b*-PAA$_{105}$/PBB-OC8 (PD3/14)	324,424	591	98
PBBCN-OC8 (15)	332,404	502	
PS$_{328}$-*b*-PAA$_{33}$/PBBCN-OC8 (PD1/15)	342,419	512	10
PS$_{304}$-*b*-PAA$_{61}$/PBBCN-OC8 (PD2/15)	360,445	595	93
PS$_{210}$-*b*-PAA$_{105}$/PBBCN-OC8 (PD3/15)	360,442	605	103
PBBOC8-OC8 (16)	399	498	
PS$_{328}$-*b*-PAA$_{33}$/PBBOC8-OC8 (PD1/16)	335,419	503	5
PS$_{304}$-*b*-PAA$_{61}$/PBBOC8-OC8 (PD2/16)	335,435	594	96
PS$_{210}$-*b*-PAA$_{105}$/PBBOC8-OC8 (PD3/16)	327,424	607	109
PBBOXD-OC8 (17)	345,409	522	
PS$_{328}$-*b*-PAA$_{33}$/PBBOXD-OC8 (PD1/17)	353,429	578	56
PS$_{304}$-*b*-PAA$_{61}$/PBBOXD-OC8 (PD2/17)	363,447	600	78
PS$_{210}$-*b*-PAA$_{105}$/PBBOXD-OC8 (PD3/17)	355,437	614	92
PBT-OC8 (18)	404	512	
PS$_{328}$-*b*-PAA$_{33}$/PBT-OC8 (PD1/18)	342,419	566	54
PS$_{304}$-*b*-PAA$_{61}$/PBT-OC8 (PD2/18)	350,442	599	87
PS$_{210}$-*b*-PAA$_{105}$/PBT-OC8 (PD3/18)	342,429	604	92
PBP-OC8 (19)	330,394	496	
PS$_{328}$-*b*-PAA$_{33}$/PBP-OC8 (PD1/19)	335,414	502	6
PS$_{304}$-*b*-PAA$_{61}$/PBP-OC8 (PD2/19)	332,396	590	94
PS$_{210}$-*b*-PAA$_{105}$/PBP-OC8 (PD3/19)	337,422	603	107

[a] Wavelength of the maximum absorbance in solid state.
[b] Wavelength of the maximum PL emission in solid state.
[c] The difference of $\lambda_{PL,film}$ between pyridyl compounds **14–19** and those after H-bonded with polymeric donors **PD1-PD3**.

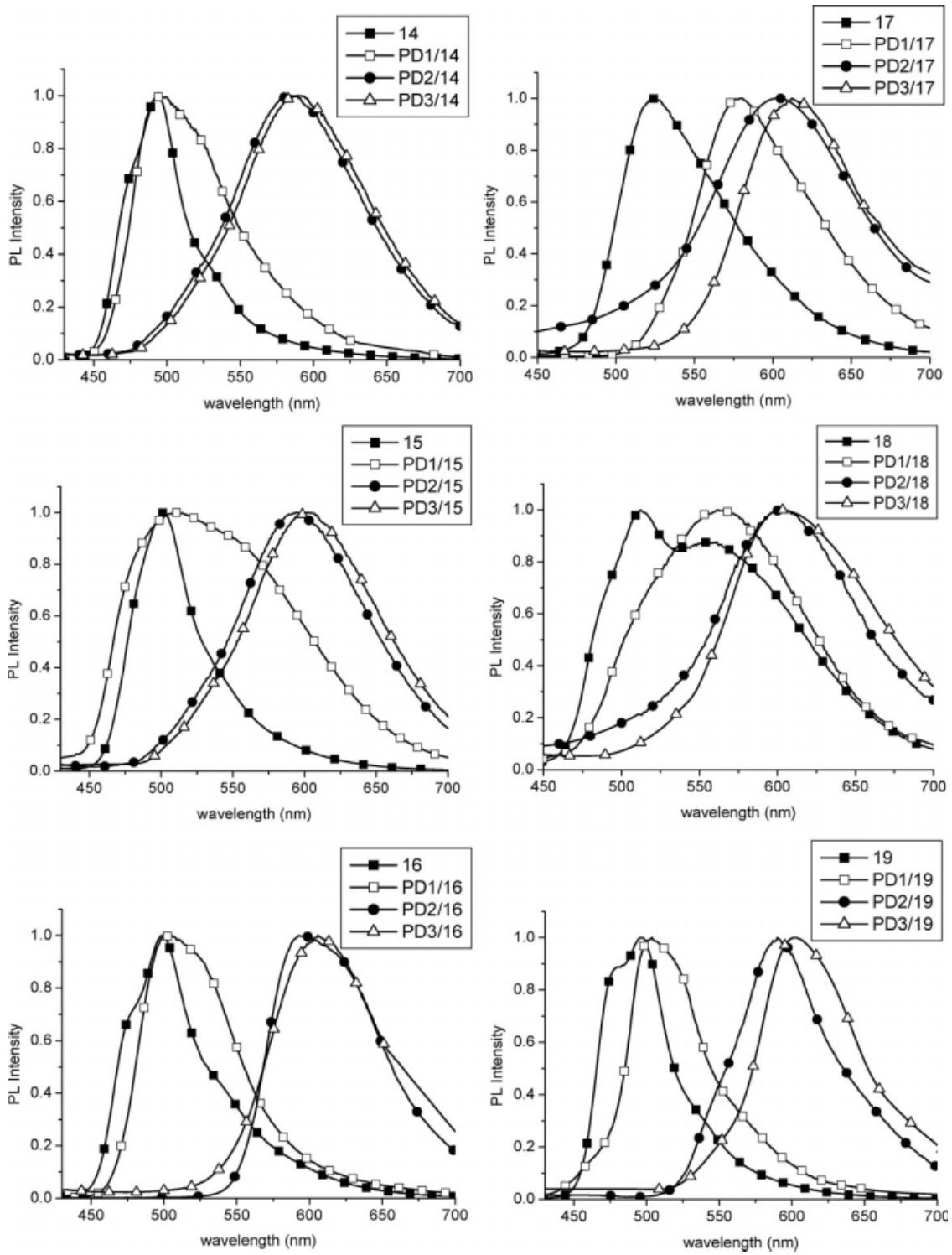

Figure 6. PL spectra of conjugated pyridyl compounds **PBB-OC$_8$** (**14**), **PBBCN-OC$_8$** (**15**), **PBBOC$_8$-OC$_8$** (**16**), **PBBOXD-OC$_8$** (**17**), **PBT-OC$_8$** (**18**), **PBP-OC$_8$** (**19**), and their H-bonded complexes with diblock copolymeric donors **PS$_{328}$-*b*-PAA$_{33}$** (**PD1**), **PS$_{304}$-*b*-PAA$_{61}$** (**PD2**), and **PS$_{210}$-*b*-PAA$_{105}$** (**PD3**) in solid films upon an excitation wavelength at 398 nm.

(c.a. $\Delta\lambda_{PL}$ = 3–10 nm), except oxadiazole- and thiophene-based pyridyl acceptors **PBBOXD-OC$_8$ (17)** and **PBT-OC$_8$ (18)** H-bonded with copolymeric donor **PS$_{328}$-*b*-PAA$_{33}$ (PD1)** (with 54–56 nm of red shifts). This phenomenon might be explained by the formation of H-bonds between the lone pairs of pyridyl units and the acidic protons contributed from **(PS-*b*-PAA)s**, and it results in lower energy band gaps of H-bonded complexes by the intramolecular charge transfer from OXD and thiophene units to pyridyl units. Besides, large difference of λ_{PL} in solid films (87–107 nm of red shifts) between pyridyl molecules and their analogous H-bonded complexes were observed in PL spectra depending on the density of H-bonds. For instance, block copolymeric donors **PS$_{304}$-*b*-PAA$_{61}$ (PD2)** and **PS$_{210}$-*b*-PAA$_{105}$ (PD3)** containing higher PAA contents have larger degrees of H-bonding, which will enhance more π–π stacking and molecular aggregation of conjugated bis-pyridyl acceptor moieties in the self-assembled complexation environment containing PAA polymeric blocks. According to these results, higher degrees of H-bonding in the double H-bonded complexes (1:2 group molar ratio of acceptor:donor) of bis-pyridyl acceptor **PBP-OC$_8$ (19)** and block copolymeric donors **(PS-*b*-PAA)s**, that is, **PD1–PD3**, revealed a greater influence on the photoluminescent behavior to exhibit longer wavelength shfits in contrast to single H-bonded complexes containing mono-pyridyl acceptor **PBB-OC$_8$ (14)/PS-b-PAA (PD1-PD3)** (1:1 group molar ratio of acceptor:donor). It is conceivable if more diblock copolymers **PD1–PD3** were fully H-bonded with bis-pyridyl **PBP-OC$_8$ (19)** in comparison with mono-pyridyl **PBB-OC$_8$ (14)**, and the polymeric donors were treated as solid solvents in the supramolecules to suppress molecular aggregation of pyridyl compounds, which will induce blue shifts of PL emissions and counteract the result of red shifts in PL emissions attributed to the H-bonded effect. However, double H-bonded complexes **(PS-*b*-PAA)s/PBP-OC$_8$ (PD1-PD3/19)** revealed slighter red shifts of PL emissions comparing with single H-bonded complexes **(PS-*b*-PAA)s/PBB-OC$_8$ (PD1-PD3/14)**, and the difference of both PL emissions show similar results by H-bonded effects. Hence, H-bonded effect is dominant than solvent dilution effect originated from larger amounts of diblock copolymeric donors. As a whole, block copolymeric donors containing higher PAA contents will have higher extents of H-bonding with mono-/bis-pyridyl acceptor emitters and followed by larger aggregations, which will induce longer red-shifted behavior of PL emissions in acceptor emitters during the H-bonded self-assembly process in solid films, i.e., $\Delta\lambda_{PL}$**(PD3/14–19)** > $\Delta\lambda_{PL}$**(PD2/14–19)** > $\Delta\lambda_{PL}$**(PD1/14–19)**, respectively.

Morphology

A set of TEM micrographs (see Fig. 7) illustrate aggregates of spherical morphologies prepared from diblock copolymer **PS$_{328}$-*b*-PAA$_{33}$ (PD1)** and its H-bonded complexes, which were incorporated with mono-pyridyl **PBB-OC$_8$ (14)** and bis-pyridyl **PBP-OC$_8$ (19)** to form H-bonded side-chain and cross-linking copolymers (**PD1/14** and **PD1/19**), respectively. As shown in Figure 7(a), the TEM image of the pure diblock copolymer **PS$_{328}$-*b*-PAA$_{33}$ (PD1)** revealed the dark region (stained with iodine) for the PAA domain and the light region for the PS domain, which is similar to the result of the literature.[36] The PAA domain exhibited spherical aggregates and micelles with diameters around 10 nm. The characterization of TEM micrograph for H-bonded complex **PS$_{328}$-*b*-PAA$_{33}$/PBB-OC$_8$ (PD1/14)** in Figure 7(b) revealed similar spherical aggregates as those **(PD1)** shown in Figure 7(a), except for the larger spherical aggregates (with diameters around 20 nm) in H-bonded complex **PD1/14**, which is larger than the self-assembled acid domains of pure donor copolymer **PD1**. Dark regions with stains represent the crystallized rod clusters of mono-pyridyl acceptor **PBB-OC$_8$** moieties H-bonded with polymeric donors PAA moieties of **PD1** in Figure 7(b), while the surrounding light regions are amorphous coil segments of the PS domains. In Figure 7(c), H-bonded complex **PS$_{328}$-*b*-PAA$_{33}$/PBP-OC$_8$ (PD1/19)**, that is, H-bonded cross-linking copolymer, has the domain size c.a. 30 nm in the dark regions, which exhibit a similar result as described in the H-bonded side-chain copolymer system. A larger amount of PAA segments were H-bonded with bis-pyridyl acceptor **PBP-OC$_8$ (19)** to form a H-bonded polymer network, which may enlarge the diameter of the cluster domain in H-bonded PAA regions. While block copolymeric donors **PS$_{304}$-*b*-PAA$_{61}$ (PD2)** and **PS$_{210}$-*b*-PAA$_{105}$ (PD3)** containing higher PAA contents have poor solubilities by preparation of TEM films from solutions of chlorobenzene due to larger degrees of H-bonding, the morphological behavior of copolymeric donors **PD2-PD3** and their H-bonded complexes were not investigated. Nevertheless, larger H-bonded self-assembled domain

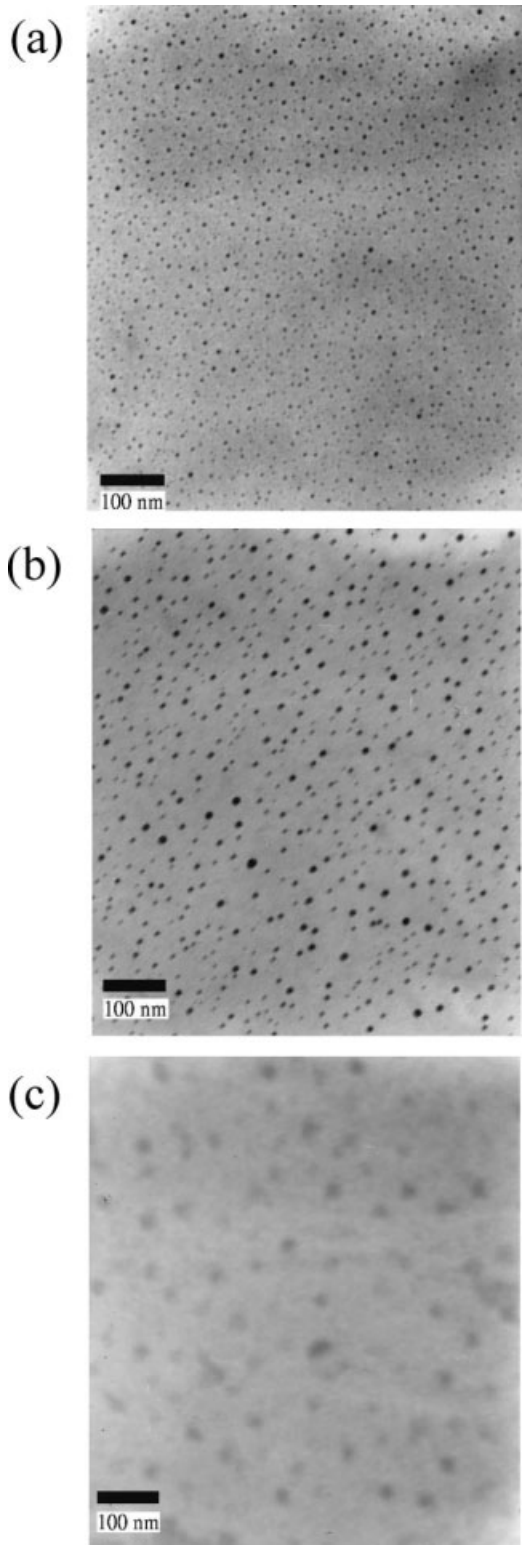

Figure 7. TEM micrographs of (a) pure diblock copolymer **PS_{328}-*b*-PAA_{33}** (**PD1**), (b) H-bonded complexes of **PS_{328}-*b*-PAA_{33}/PBB-OC_8** (**PD1/14**), and (c) **PS_{328}-*b*-PAA_{33}/PBP-OC_8** (**PD1/19**).

sizes can be expected in analogous H-bonded complexes of **PD2-PD3** in contrast to the H-bonded complexes of **PD1**.

Electrochemical Properties

To analyze the energy band structures of PLED devices, the energy levels of the highest occupied molecular orbital (HOMO) and the lowest unoccupied molecular orbital (LUMO) of all components were characterized by the cyclic voltammetry (CV) in a conventional three-electrode cell to investigate the redox behavior in solid films. The potentials estimated here were based on the following equation reported by de Leeuw et al.,[37] $E^{HOMO}/E^{LUMO} = -(E^{ox,onset}/E^{red,onset} + 4.4$ eV), where $E^{ox,onset}$ and $E^{red,onset}$ were the onset potentials for the oxidation and reduction processes of a polymer vs. saturated calomel electrode (SCE). The onset potentials were determined from the intersection of two tangents drawn at the rising and background currents of the CV curves. Because the reduction curves of polymers were not observed, crude estimations of the LUMO levels of reduction polymers were deduced from the HOMO values and the optical band gaps from the edges of the longest absorption bands in the absorption spectra. The measured oxidation potentials and HOMO/LUMO energy values are summarized in Table 4. The H-bonded side-chain and cross-linking copolymers **PD1/16–19** show the onset potentials of oxidation between 0.91 and 1.01 V in the anodic scans. Compared with **PBBOC_8-OC_8 (16)**, the oxadiazole and bis-pyridyl moieties in **PBBOXD-OC_8 (17)** and **PBP-OC_8 (19)** act as electron-withdrawing substituents and thus to decrease the LUMO levels.

Table 4. HOMO and LUMO Energies and Electrochemical Properties of H-Bonded Complexes (**PD1/16–19**)

H-Bonded Complexes	$E^{ox,onset}$ (V)	E^{HOMO} (eV)[a]	E^{LUMO} (eV)[b]	E^{opt} (eV)[c]
PD1/16	0.97	−5.37	−2.86	−2.51
PD1/17	0.92	−5.32	−2.91	−2.41
PD1/18	0.91	−5.31	−2.87	−2.44
PD1/19	1.01	−5.41	−2.94	−2.47

[a] HOMO Energies were obtained from the cyclic voltammetry.
[b] LUMO Energies were deduced from the HOMO values and optical band gaps.
[c] Optical band gaps were obtained from the UV-vis absorption spectra.

Table 5. PL Properties of H-Bonded Complexes (PD1/16, PD1/18, and PD1/19) and EL Data of Their PLED Devices[a]

H-Bonded Complexes	$\lambda_{max,PL}$ (nm)[b]	$\lambda_{max,PL}$ (nm)[c]	$\lambda_{max,EL}$ (nm)	V_{on} (V)[d]	Power Efficiency (cd/A)[e]	Max. Luminescence (cd/m^2)
PD1/16	503	491	508	7.5	0.30	322
PD1/18	566	560	560	8.0	0.37	519
PD1/19	502	494	503	9.0	0.23	318

[a] Device configuration: ITO/PEDOT:PSS/H-bonded complexes/BCP/Alq_3/LiF/Al.
[b] Wavelength of the maximum PL emission of spin-coated thin film from THF.
[c] Wavelength of the maximum PL emission of spin-coated thin film from chlorobenzene.
[d] V_{on} is the turn on voltage of light.
[e] Power efficiency were obtained at 100 mA/cm^2.

Besides, with respect to H-bonded complex **PD1/16** (HOMO = −5.37 eV and LUMO = −2.86 eV), the oxadiazole- and thiophene-based emitters **PBBOXD-OC_8 (17)** and **PBT-OC_8 (18)** in **PS_{328}-*b*-PAA_{33} (PD1)** polymer matrix show higher HOMO levels (−5.32 and −5.31 eV) and lower LUMO levels (−2.91 and −2.87 eV), so H-bonded complexes **PD1/17–18** possess smaller band gaps along with longer wavelength emissions.

Electroluminescent (EL) Properties of PLED Devices

H-bonded complexes **PD1/16, PD1/18, and PD1/19** were fabricated into four-layer PLED devices, respectively, with a configuration of ITO/PEDOT:PSS(40–50 nm)/H-bonded complexes (50–60 nm)/BCP(10 nm)/Alq_3(30 nm)/LiF(1 nm)/Al(150 nm) using standard procedures of spin-coating (with a concentration of 10 mg/mL in chlorobenzene) and vacuum deposition methods, and the EL properties are demonstrated in Table 5. PEDOT:PSS, H-bonded complexes **PD1/16, PD1/18, and PD1/19**, 2,9-dimethyl-4,7-diphenyl-1,10-phenanthroline (BCP), and Alq_3 were used as hole transporting, emission, hole blocking (to block holes away from the Alq_3 layer completely), and electron transporting layers, respectively.[38] Under a bias voltage, the PLED devices showed green emissions with $\lambda_{max,EL}$ in the range of 503–560 nm (as shown in Fig. 8). The current-voltage and luminescence-voltage curves of all PLED devices are displayed in Figure 9. The turn-on voltages of these PLED devices were about 7.5–9.0 V, and their power efficiencies and maximum luminances were 0.23–0.37 cd A^{-1} (at 100 $mAcm^{-2}$) and 318–519 cdm^{-2} (at around 25 V), respectively. As shown in Table 5, comparing the results of the maximum efficiencies and luminances for all PLED devices, we can conclude that the enhanced EL performance

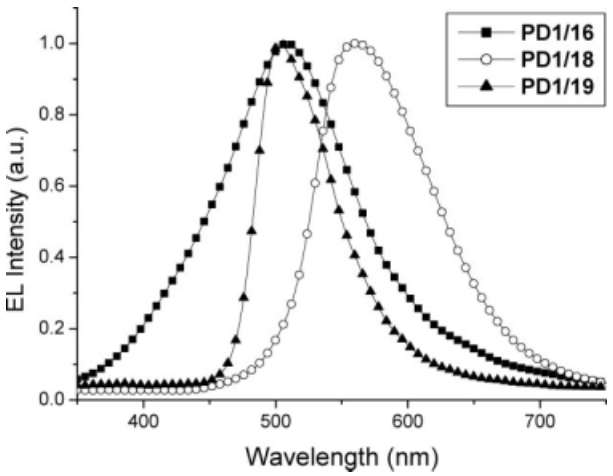

Figure 8. EL spectra of PLED devices with the configuration of **ITO/PEDOT:PSS**/H-bonded complexes(**PD1/16**, **PD1/18**, and **PD1/19**)/**BCP/Alq_3/LiF/Al**.

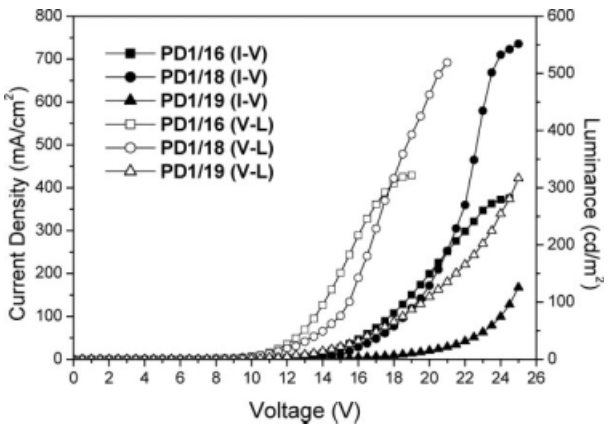

Figure 9. Current-voltage-luminance (I-V-L) characteristics of PLED devices with the configuration of **ITO/PEDOT:PSS**/H-bonded complexes(**PD1/16**, **PD1/18**, and **PD1/19**)/**BCP/Alq_3/LiF/Al**.

of the PLED devices with higher efficiencies and luminances can be achieved by the incorporation of thiophene units into the pyridyl emitters, that is, **PBT-OC$_8$ (18)**, in the light-emitting H-bonded supramolecular systems. However, the worst EL behavior (highest turn-on voltage, lowest power efficiency, and lowest max. luminance) in the PLED device of H-bonded complex **PD1/19** may be due to the intrinsic insulation property of the higher extent of H-bonding by the double H-bonded complexation between pyridyl **PBP-OC$_8$ (19)** and **PS$_{328}$-*b*-PAA$_{33}$ (PD1)** (acceptor:donor = 1:2 in group molar ratio), where the largest aggregation of emitters occurred in the double H-bonded complexation of **PD1/19** was also previously confirmed by the morphology of TEM photographs. As shown in Figure 8 and Table 5, the EL emission peaks of the PLED devices are slightly red shifted than PL emission peaks. In general, the EL emission peaks of all PLED devices are well matched with their corresponding PL emission peaks of the solid films.

CONCLUSIONS

The self-assembled matrix of micellar diblock copolymers **(PS-*b*-PAA)s** were hydrolyzed from diblock copolymers **(PS-*b*-P*t*BuA)s**, in which tert-butyl acrylate group were turn into acrylic acid groups by hydrolysis reaction. Accordingly, a series of photoluminescent mono- and bis-pyridyl acceptors were designed to complex with amphiphilic diblock copolymers **(PS-*b*-PAA)s** to form single/double H-bonded complexes, that is, supramolecular side-chain/cross-linking polymers, respectively. Therefore, H-bonded effects on the self-assembled and PL properties of these supramolecules in solid state are illustrated. The diblock copolymers **(PS-*b*-P*t*BuA)s** with different styrene molar ratios (10/1, 5/1, and 2/1) were synthesized and their derivatives **(PS-*b*-PAA)s** demonstrated adverse (worse) thermal properties after hydrolysis. By increasing the proportion of P*t*BuA and PAA constituents in block copolymers **(PS-*b*-P*t*BuA)s** and **(PS-*b*-PAA)s**, their glass transition temperatures were enhanced but their thermal stabilities were reduced. In the H-bonded complexes of **(PS-*b*-PAA)s** (with different amounts of PAA contents) and various conjugated pyridyl emitters, the original melting points of pyridyl molecules and T_g transitions of block copolymers were not observed, which confirmed the complete formation of H-bonded complexes. In addition, large red-shifted PL emissions (e.g., $\Delta\lambda_{PL,max}$ = 109 nm) of supramolecular H-bonded architectures were obtained by increasing the PAA content of the surrounding diblock copolymeric donors so as to increase the degree of H-bonding. As evidenced by TEM micrographs, the H-bonded complexes exhibited self-assembled morphology of spherical micelle-like structures with various diameters, which corresponded to the aggregates of pyridyl acceptors surrounded by PAA donor constituents of block-copolymers. PLED devices with the configuration of ITO/PEDOT:PSS/H-bonded complexes/BCP/Alq_3/LiF/Al were fabricated to emit green light. The EL efficiencies were improved by the incorporation of thiophene units into pyridyl acceptors, and the EL properties were also correlated to their nanostructural morphology.

The authors express their sincere thanks to the National Center for High-performance Computing for computer time and facilities. They also acknowledge the financial supports of this project provided by the National Science Council of Taiwan (ROC) through NSC 96-2113M-009-015, National Chiao Tung University through 97W807, and Chung-Shan Institute of Science and Technology (in Taiwan). The instrumental support of vacuum deposition was provided by Prof. Yu-Tai Tao at Institute of Chemistry, Academia Sinica (in Taiwan).

REFERENCES AND NOTES

1. (a) Gao, L.; Shi, L.; An, Y.; Zhang, W.; Shen, X.; Guo, S.; He, B. Langmuir 2004, 20, 4787–4790; (b) Goh, S. L.; Platt, A. P.; Rutledge, K. E.; Lee, I. J Polym Sci Part A: Polym Chem 2008, 46, 5381–5389; (c) Qiu, S.; Huang, H.; Dai, X. H.; Zhou, W.; Dong, C. M. J Polym Sci Part A: Polym Chem 2009, 47, 2009–2023.
2. (a) Yoshida, E.; Kunugi, S. Macromolecules 2002, 35, 6665–6669; (b) Wang, S.; Zhou, H.; Dang, G.; Chen, C. J Polym Sci Part A: Polym Chem 2009, 47, 2024–2031; (c) Deepa, P.; Jayakannan, M. J Polym Sci Part A: Polym Chem 2008, 46, 5897–5915; (d) Vera, F.; Almuzara, C.; Orera, I.; Barberá, J.; Oriol, L.; Serrano, J. L.; Sierra, T. J Polym Sci Part A: Polym Chem 2008, 46, 5528–5541.
3. (a) Hofmeier, H.; Schubert, U. S. Macromol Chem Phys 2003, 204, 1391–1397; (b) Han, F. S.; Higuchi, M.; Ikeda, T.; Negishi, Y.; Tsukuda, T.; Kurth, D. G. J Mater Chem 2008, 18, 4555–4560; (c) Vellis, P. D.; Mikroyannidis, J. A.; Lo, C. N.; Hsu C. S. J Polym Sci Part A: Polym Chem 2008, 46, 7702–7712.

4. (a) Zhang, W.; Shi, L.; An, Y.; Shen, X.; Guo, Y.; Gao, L.; Liu, Z.; He, B. Langmuir 2003, 19, 6026–6031; (b) Watanabe, R.; Kamata, K.; Iyoda, T. J Mater Chem 2008, 18, 5482–5491; (c) Lin, S. T.; Tung, Y. C.; Chen, W. C. J Mater Chem 2008, 18, 3985–3992.
5. (a) Cornelissen, J. J. L. M.; Fischer, M.; Sommerdijk, N. A. J. M.; Nolte, R. J. M. Science 1998, 280, 1427–1430; (b) Liang, Y. G.; Wang, H. B.; Yuan, S. W.; Lee, Y. G.; Gan, L.; Yu, L. P. J Mater Chem 2007, 17, 2183–2194.
6. Schlaad, H.; Krasia, T.; Antonietti, M. J Am Chem Soc 2004, 126, 11307–11310.
7. Schlaad, H.; Smarsly, B.; Below, I. Macromolecules 2006, 39, 4631–4632; (b) Patil, A. J.; Mann, S. J Mater Chem 2008, 18, 4605–4615.
8. Uzun, O.; Frankamp, B. L.; Sanyal, A.; Rotello, V. M. Chem Mater 2006, 18, 5404–5409; (b) Lim, Y. b.; Moon, K. S.; Lee, M. J Mater Chem 2008, 18, 2909–2918.
9. Liu, S.; Zhu, H.; Zhao, H.; Jiang, M.; Wu, C. Langmuir 2000, 16, 3712–3717.
10. Ma, N.; Zhang, H.; Song, B.; Wang, Z.; Zhang, X. Chem Mater 2005, 17, 5065–5069.
11. Peng, H.; Chen, D.; Jiang, D. Langmuir 2003, 19, 10989–10992.
12. (a) Zhang, W.; Shi, L.; An, Y.; Wu, K.; Gao, L.; Liu, Z.; Ma, R.; Meng, Q.; Zhao, C.; He, B. Macromolecules 2004, 37, 2924–2929; (b) Wen, F.; Zhang, W.; Zheng, P.; Zhang, X.; Yang, X.; Wang, Y.; Jiang, X.; Wei, G.; Shi, L. J Polym Sci Part A: Polym Chem 2008, 46, 1192–1202.
13. Chen, D.; Jiang, M. Acc Chem Res 2005, 38, 494–502.
14. Tjandra, W.; Yao, J.; Ravi, P.; Tam, K. C.; Alamsjah, A. Chem Mater 2005, 17, 4865–4872.
15. (a) Kanie, K.; Nishii, M.; Yasuda, T.; Taki, T.; Ujiie, S.; Kato, T. J Mater Chem 2001, 11, 2875–2886; (b) Yu, H. F.; Shishido, A.; Li, J. Z.; Kamata, K.; Iyoda, T.; Ikeda, T. J Mater Chem 2007, 17, 3485–3488.
16. Osuji, C.; Chao, C. Y.; Bita, I.; Ober, C. K.; Thomas, E. L. Adv Funct Mater 2002, 12, 753–758.
17. Kato, T.; Mizoshita, N.; Kishimoto, K. Angew Chem Int Ed Engl 2006, 45, 38–68.
18. (a) Lin, H. C.; Tsai, C. M.; Huang, G. H.; Tao, Y. T. Macromolecules 2006, 39, 557–568; (b) Xu, J.; Ling, T. C.; He, C. J Polym Sci Part A: Polym Chem 2008, 46, 4691–4703.
19. Xue, C.; Jin, S.; Weng, X.; Ge, J. J.; Shen, Z.; Shen, H.; Graham, M. J.; Jeong, K. U.; Huang, H.; Zhang, D.; Guo, M.; Harris, F. W.; Cheng, S. Z. D. Chem Mater 2004, 16, 1014–1025.
20. Kohlmeier, A.; Janietz, D. Chem Mater 2006, 18, 1483–1489.
21. Tang, C.; Lennon, E. M.; Fredrickson, G. H.; Kramer, E. J.; Hawker, C. J. Science 2008, 322, 429–432.
22. (a) Zhang, W.; Shi, L.; Gao, L.; An, Y.; Wu, K. Macromol Rapid Commun 2005, 26, 1341–1345; (b) Zhang, W.; Shi, L.; Gao, L.; An, Y.; Li, G.; Wu, K.; Liu, Z. Macromolecules 2005, 38, 899–903; (c) Mendrek, S.; Mendrek, A.; Adler, H. J.; Dworak, A.; Kuckling, D. J Polym Sci Part A: Polym Chem 2009, 47, 1782–1794.
23. Zhang, W.; Shi, L.; Miao, Z. J.; Wu, K.; An, Y. Macromol Chem Phys 2005, 206, 2354–2361.
24. Zhang, L.; Eisenberg, A. Macromolecules 1996, 29, 8805–8815.
25. Zhang, L.; Eisenberg, A. Macromolecules 1999, 32, 2239–2249.
26. Yu, Y.; Eisenberg, A. J Am Chem Soc 1997, 119, 8383–8324.
27. Kang, Y.; Taton, T. A. J Am Chem Soc 2003, 125, 5650–5651.
28. Lin, H. C.; Lin, Y. S.; Lin, Y. S.; Chen, Y. T.; Chao, I.; Li, T. W. Macromolecules 1998, 31, 7298–7311; (b) Lin, H. C.; Sheu, H. Y.; Chang, C. L.; Tsai, C. J Mater Chem 2001, 11, 2875–2886; (c) Lin, H. C.; Hendrianto, J. Polymer 2005, 46, 12146–12157; (d) Wu, C. W.; Lin, H. C. Macromolecules 2006, 39, 7985–7997.
29. (a) Jenekhe, S. A.; Chen, X. L. Science 1999, 283, 372–375; (b) Chen, X. L.; Jenekhe, S. A. Langmuir 1999, 15, 8007–8017.
30. Bockstaller, M. R.; Mickiewicz, R. A.; Thomas, E. L. Adv Mater 2005, 17, 1331–1349.
31. Meng, H.; Chen, Z. K.; Huang, W. J Phys Chem B 1999, 103, 6429–6433.
32. (a) Hautekeer, J. P.; Varshney, S. K.; Fayt, R.; Jacobs, C.; Jerome, R.; Teyssie, P. H. Macromolecules 1990, 23, 3893–3898; (b) Pralle, M. U.; Whitaker, C. M.; Braun, P. V.; Stupp, S. I. Macromolecules 2000, 33, 3550–3556.
33. Kong, H.; Gao, C.; Yan, D. J Mater Chem 2004, 14, 1401–1405.
34. Wang, L.; Fu, Y.; Wang, Z.; Fan, Y.; Zhang, X. Langmuir 1999, 15, 1360–1363.
35. Zhang, H. Y.; Wang, Z. Q.; Zhang, Y. Q.; Zhang, X. Langmuir 2004, 20, 9366–9370; (b) O'Neal, K. L.; Geib, S.; Weber, S. G. Anal Chem 2007, 79, 3117–3125.
36. Zhang, L.; Eisenberg, A. J Am Chem Soc 1996, 118, 3168–3181.
37. De Leeuw, D. M.; Simenon, M. M. J.; Brown, A. R.; Einerhand, R. E. F. Synth Met 1997, 87, 53–59.
38. Chen, C. T.; Wei, Y.; Lin, J. S.; Moturu, M. V. R. K.; Chao, W. S.; Tao, Y. T.; Chien, C. H. J Am Chem Soc 2006, 128, 10992–10995.